Fluctuations in electron-positron plasmas: Linear theory and implications for turbulence

S. Peter Gary*

Los Alamos National Laboratory, Los Alamos, NM 87545

Homa Karimabadi†

Department of Electrical and Computer Engineering,

University of California, San Diego, La Jolla, CA 92093

(Dated: March 5, 2009)

Abstract

Linear kinetic theory of electromagnetic fluctuations in a homogeneous, magnetized, collisionless electron-positron plasma predicts two lightly damped modes propagate at relatively long wavelengths: an Alfvén-like mode with dispersion $\omega_r = k_{\|}\tilde{v}_A$ and a magnetosonic-like mode with dispersion $\omega_r \simeq k\tilde{v}_A$ if $\beta_e << 1$. Here $\tilde{v}_A$ is the Alfvén speed in an electron-positron plasma and $\|$ refers to the direction relative to the background magnetic field $\mathbf{B}_o$. Both modes have phase speeds ω_r/k which monotonically decrease with increasing wavenumber. The Alfvén-like fluctuations are almost incompressible, but the magnetosonic-like fluctuations become strongly compressible at short wavelengths and propagation sufficiently oblique to $\mathbf{B}_o$. Using the linear dispersion properties of these modes, scaling relations are derived which predict that turbulence of both modes should be relatively anisotropic, with fluctuating magnetic energy preferentially cascading in directions perpendicular to $\mathbf{B}_o$. Turbulent spectra in the solar wind show two distinct power-law regimes separated by a distinct breakpoint in observed frequency; this characteristic should not be present in electron-positron turbulence because of the absence of whistler-like dispersion. Linear theory properties of the cyclotron and mirror instabilities driven by either electron or positron temperature anisotropies are generally analogous to those of the corresponding instabilities in electron-proton plasmas.

I. INTRODUCTION

Most computational studies of homogeneous turbulence in magnetized, collisionless plasmas have utilized fluid models such as magnetohydrodynamics (MHD) [References [1] and [2] and citations therein] and electron magnetohydrodynamics (EMHD). [3], [4], [5] However, collisionless dissipation usually increases with increasing wavenumber k, so that a kinetic approach is necessary to provide a complete description of short-wavelength turbulence such as that due to whistler fluctuations in collisionless plasmas. Particle-in-cell (PIC) simulations, which represent both electrons and ions as super-particles, capture not only the wave-wave interactions represented by fluid descriptions, but also the wave-particle interactions such as Landau and cyclotron damping which describe the dissipation of plasma turbulence cascading to short wavelengths. Current computing facilities do not yet allow long-time simulations of plasma turbulence with physically realistic proton-electron mass ratios. But substantial simulations of turbulence in electron-positron plasmas do lie within the realm of current capability. Thus electron-positron PIC models can be powerful tools for testing predictions drawn from fundamental theories of plasma turbulence and magnetic reconnection [6], [7], [8], [9].

The first PIC simulation of whistler turbulence[10] demonstrated the forward cascade of such fluctuations from relatively long to shorter wavelengths, and also showed that such turbulence becomes anisotropic with more energy at directions of propagation relatively perpendicular to the background magnetic field $\mathbf{B}_o$ as contrasted with directions relatively parallel to $\mathbf{B}_o$. Saito *et al.* [11] carried out further PIC simulations of whistler turbulence, showing that the turbulence becomes more anisotropic as the fluctuation amplitudes increase, and deriving scaling arguments which predict an anisotropy consistent with that obtained from the computations.

Theories of fluctuations in electron-positron plasmas may also be applied to astrophysical plasmas. The high-energy radiation environments of some astrophysical objects may maintain an electron-positron plasma through pair creation and annihilation; under such circumstances relativistic theories [12], [13], [14], [15], [16] and simulations [17] must be used. However, the research described in this manuscript addresses only non-relativistic plasmas; this enables us to examine the complete kinetic dispersion equation for homogeneous, collisionless plasmas without any approximations beyond that of small-amplitude

linear theory.

It has been hypothesized that weak homogeneous turbulence in collisionless, magnetized plasmas reflects the properties of its constituent small-amplitude fluctuations. In the framework of this hypothesis, we here use linear theory of electromagnetic fluctuations to predict basic properties of turbulence in electron-positron plasmas as a preface for future PIC simulations of such turbulence.

Therefore, we here consider the linear kinetic theory of fluctuations in electron-positron plasmas, and use the results to construct scaling relations analogous to those of Reference [11]. If the electron and positron temperatures are similar, electrostatic fluctuations at frequencies below the plasma frequency are heavily damped, so we here address only electromagnetic fluctuations. If the wavevector $\mathbf{k}$ satisfies $\mathbf{k} \times \mathbf{B}_o = 0$, Iwamoto [18] used linear kinetic theory to show that the left-hand and right-hand circularly polarized fluctuations have identical dispersion, and, as a consequence, the whistler mode does not exist in electron-positron plasmas. Here we consider the more general case of propagation oblique to $\mathbf{B}_o$; we find two distinct electromagnetic modes in an isotropic electron-positron plasma, analogous to the Alfvén and magnetosonic modes of an electron-proton plasma; we label them the Alfvén-like and magnetosonic-like modes. We find that both modes are relatively free of dispersion in the wavenumber regime of weak damping; this stands in contrast to the strongly dispersive fluctuations found on magnetosonic-whistler modes in electron-proton plasmas. Thus electron-positron PIC simulations should enable the study of kinetic dissipation in plasmas in the absence of whistler-like dispersion.

Section II of this manuscript describes some linear theory properties of these two modes. Section III uses these linear properties to predict some properties of turbulence in electron-positron plasmas. Section IV describes linear theory properties of the cyclotron and mirror instabilities driven by temperature anisotropies on either the electrons or the positrons. Section V draws conclusions from our research.

We denote the jth species plasma frequency as $\omega_j \equiv \sqrt{4\pi n_j e_j^2/m_j}$, the jth species cyclotron frequency as $\Omega_j \equiv e_j B_o/m_j c$, and $\beta_{\|j} \equiv 8\pi n_j k_B T_{\|j}/B_o^2$. Solutions to the linear dispersion equation are in terms of a wavevector $\mathbf{k}$ with real components and a complex frequency $\omega = \omega_r + i\gamma$. The symbols $\|$ and $\perp$ denote directions parallel and perpendicular, respectively, to the background magnetic field $\mathbf{B}_o$, and the subscripts e and p will refer to electron and positron, respectively. Here the Alfvén speed in an electron-positron plasma is

$\tilde{v}_A \equiv B_o/\sqrt{8\pi n_e m_e}$. We define θ, the angle of mode propagation, by $\mathbf{k} \cdot \mathbf{B}_o = kB_o \cos(\theta)$.

II. LINEAR THEORY

This section describes results from the solution of the linear kinetic dispersion equation for electromagnetic fluctuations in a homogeneous, collisionless electron-positron plasma. Unless stated otherwise, the dimensionless parameters characterizing the zeroth order background plasma are $\beta_{\|e} = 0.10$, $\omega_e/|\Omega_e| = 2.5$, $T_e = T_p$, $T_{\perp j} = T_{\|j}$, and $m_e = m_p$. Our results are essentially independent of $\omega_e/|\Omega_e|$ as long as this parameter is much greater than unity. We choose $\omega_e/|\Omega_e| = 2.5$ for our calculations because PIC simulations run most efficiently when $\omega_e/|\Omega_e|$ is of order unity. We assume the zeroth order velocity distribution of each species to be a Maxwellian or bi-Maxwellian, and solve the full electromagnetic dispersion equation[19] without analytic approximation.

Linear theory yields two distinct electromagnetic modes, which we call the Alfvén-like and magnetosonic-like modes, with linear dispersion properties illustrated in Figures 1 and 2. At $\mathbf{k} \times \mathbf{B}_o = 0$, the two modes have identical dispersion and damping, with $\omega_r = k\tilde{v}_A$ and essentially zero damping at $kc/\omega_e << 1$. At parallel propagation, the Alfvén-like mode is left-hand circularly polarized, and the magnetosonic-like mode is right-hand circularly polarized. At shorter wavelengths, the cyclotron resonances assert themselves (positron cyclotron resonance for the Alfvén-like mode and the electron cyclotron resonance for the magnetosonic-like mode), ω_r becomes dispersive, and cyclotron damping displays its characteristic rapid onset as $k_{\|}c/\omega_e$ approaches unity.

At propagation oblique to $\mathbf{B}_o$, however, the properties of the two modes diverge; the Alfvén-like mode shown in Figure 1 satisfies $\omega_r = k_{\|}\tilde{v}_A$ at long wavelength, whereas the magnetosonic-like mode shown in Figure 2 is more nearly isotropic with $\omega_r \simeq k\tilde{v}_A$ at $kc/\omega_e << 1$. Both modes have phase speeds ω_r/k which monotonically decrease with increasing wavenumber, so that neither mode exhibits whistler-like dispersion.[18] For the $\beta_e = 0.10$ case illustrated here, damping of both modes has significant onset at $k_{\|}c/\omega_e \sim 1$.

The differences in dispersion between the two modes are relatively small, so for diagnostic purposes it is useful to consider other quantities which have larger differences in numerical value. We here examine several "transport ratios", ratios of the squares of fluctuating quantities which are independent of fluctuation amplitude and can be readily computed

from linear theory [e.g., Reference [19], Chapter 5]. The three quantities of interest here are the magnetic compressibility

$$C_{\|} \equiv \frac{|\delta B_{\|}|^2}{|\delta \mathbf{B}|^2} \quad ,$$

the parallel fluctuating electric field ratio

$$\frac{|\delta E_{\|}|^2}{|\delta \mathbf{E}|^2} \quad ,$$

and the jth species compressibility

$$C_j \equiv \frac{|\delta n_j|^2}{n_j^2} \frac{B_o^2}{|\delta \mathbf{B}|^2} \quad .$$

In electron-positron plasmas both the Alfvén-like and magnetosonic-like modes have zero magnetic compressibility for all wavevectors illustrated in Figures 1 and 2. In contrast the magnetic compressibility in electron-proton plasmas is non-zero for both kinetic Alfvén and magnetosonic modes; although $C_{\|} << 1$ for the former mode at $\beta_e = 0.10$ [Reference [20], Figure 7], the latter mode can exhibit $C_{\|}$ close to unity at sufficiently oblique propagation.

Although the magnetic compressibility is zero, the parallel fluctuating electric fields in electron-positron plasmas are not. Figure 1b and Figure 2b show that $|\delta E_{\|}|^2/|\delta \mathbf{E}|^2 << 1$ for both modes; the same condition holds for the kinetic Alfvén and magnetosonic modes in an electron-proton plasma [e.g., Fig. 7 of Reference [20]].

At oblique propagation the electron and positron compressibilities are non-zero and equal for both Alfvén-like and magnetosonic-like fluctuations. However, as shown in Figures 1c and 2c, $C_p << 1$ for the former mode, whereas $C_p \gtrsim 1$ at sufficiently oblique angles of propagation and sufficiently large kc/ω_e of the latter mode. Similar relationships hold for kinetic Alfvén and magnetosonic fluctuations at $m_p = 1836 m_e$.

Figure 3 illustrates the $\beta_{\|p}$ dependence of dispersion and damping for the Alfvén-like mode at parallel propagation. With increasing $\beta_{\|p}$, the mode shows stronger departures from $\omega_r = k_{\|}\tilde{v}_A$ at short wavelengths, and the onset of positron cyclotron damping takes place at smaller values of $k_{\|}c/\omega_e$. The same figure applies to the magnetosonic-like mode at $\mathbf{k} \times \mathbf{B}_o = 0$ if $\beta_{\|e}$ and $\beta_{\|p}$ are interchanged. As $\beta_{\|e}$ increases, that mode shows stronger dispersion and the onset of electron cyclotron damping is at smaller values of $k_{\|}c/\omega_e$. At $\mathbf{k} \times \mathbf{B}_o = 0$ the magnetosonic-like mode is relatively independent of variations in $\beta_{\|p}$, and the Alfvén-like mode is similarly independent of variations in $\beta_{\|e}$. Note that, even for $T_e \neq T_p$, there is no evidence for whistler-like (i.e. $\omega_r \simeq k^2$) dispersion for either mode.

III. SCALING RELATIONS

This section uses the results of Section II to construct a scenario for cascading weak turbulence in a homogeneous electron-positron plasma. Our two fundamental assumptions are, first, that linear dispersion and dissipation determine the characteristics of such turbulence [21] and, second, that some nonlinear properties of the turbulence follow from arguments parallel to those applied to weak whistler turbulence. [5], [11], [22], [23]

Observations [24] show two distinct regimes of solar wind turbulence spectra: the long-wavelength inertial range with $|\delta\mathbf{B}|^2 \sim k^{-\alpha}$ with $\alpha \simeq 5/3$, and a shorter wavelength regime with $\alpha > 5/3$ often termed the "dissipation range". The breakpoint between the two regimes lies approximately at $kc/\omega_{proton} \simeq 1$. Reference [21] attributes this breakpoint to the transition from Alfvén-like dispersion ($\omega_r \simeq kv_A$) at longer wavelengths to whistler-like dispersion at shorter wavelengths. Another scenario attributes the properties of the dissipation range to the predominance of oblique-propagating kinetic Alfvén waves. [25], [26] Although the controversy continues as to whether whistlers or kinetic Alfvén waves are the primary constituent of the short-wavelength regime of solar wind turbulence, both modes exhibit quadratic dispersion ($\omega_r \sim k^2$) at short wavelengths, and it is plausible to assume that the steep power-law spectra at high frequencies are due to such dispersion.[21] On the basis of this assumption, and in the absence of any quadratic dispersion for either the Alfvén-like or magnetosonic-like modes, we predict no breakpoint in homogeneous electron-positron turbulence. PIC simulations should show only a relatively steep ($\alpha > 5/3$) power law spectrum in the cascade regime, followed by a true dissipation range with a faster-than-power-law spectral decrease at $kc/\omega_e > 1$ as predicted by Reference [27].

Next, we consider the interaction of wave packets with parallel widths $l_\parallel = 2\pi/k_\parallel$ where the constituent modes each satisfy either the Alfvén-like dispersion equation $\omega_r \simeq k_\parallel \tilde{v}_A$ or the low-β magnetosonic-like $\omega_r \simeq k\tilde{v}_A$. The wave packet interaction time τ_w is determined by fluctuation properties at propagation parallel to $\mathbf{B}_o$, so

$$\tau_w \simeq \frac{l_\parallel}{(\partial\omega/\partial k_\parallel)} \tag{1}$$

For an eddy of scale length l the turnover time is $\tau_{eddy} \simeq l/\delta v_e$ where the denominator is the fluctuating electron velocity from the EMHD model. Then

$$\tau_{eddy} \simeq \frac{2\pi}{|\Omega_e|}\frac{\omega_e^2}{k^2c^2}\frac{B_o}{|\delta\mathbf{B}|} \tag{2}$$

Following the usual assumption of weak incoherent interactions between eddies, the time scale for the cascade of turbulent fluctuation energy is

$$\tau_{cascade} \equiv \frac{\tau_{eddy}^2}{\tau_w} \tag{3}$$

In strong turbulence, Alfvén-like fluctuations and magnetosonic-like fluctuations are tightly coupled. But if amplitudes are sufficiently weak, it is possible that the two modes are only weakly interactive, and that turbulence associated with each mode can be treated separately. The following arguments are based upon this assumption.

First consider Alfvén-like fluctuations with

$$\tau_w(\mathbf{k}) \simeq \frac{2\pi}{k_{\|}\tilde{v}_A}$$

Then the cascade time is

$$\tau_{cascade}(\mathbf{k}) \simeq \frac{2\pi}{|\Omega_e|}\frac{k_{\|}}{\sqrt{2}k}\frac{\omega_e^3}{k^3c^3}\frac{B_o^2}{|\delta\mathbf{B}(\mathbf{k})|^2} \tag{4}$$

Second, consider interacting magnetosonic-like wave packets with low-β dispersion $\omega_r \simeq k\tilde{v}_A$; then

$$\tau_w(\mathbf{k}) \simeq \frac{2\pi}{k_{\|}\tilde{v}_A}\frac{k}{k_{\|}}$$

It follows that the cascade time is

$$\tau_{cascade}(\mathbf{k}) \simeq \frac{2\pi}{|\Omega_e|}\frac{k_{\|}^2}{\sqrt{2}k^2}\frac{\omega_e^3}{k^3c^3}\frac{B_o^2}{|\delta\mathbf{B}(\mathbf{k})|^2} \tag{5}$$

We consider two cases: Case I with $k_\perp >> k_{\|}$, and Case II with $k_\perp << k_{\|}$. We also make two assumptions: first, that the $k_\perp$ of Case I is of the same order as $k_{\|}$ of Case II, and, second, that $|\delta\mathbf{B}(k_\perp)|^2 \sim |\delta\mathbf{B}(k_{\|})|^2$. Then for the Alfvén-like fluctuations it follows that

$$\frac{\tau_{cascade}(k_\perp)}{\tau_{cascade}(k_{\|})} \simeq \left(\frac{k_{\|}}{k_\perp}\right)_I << 1$$

Similarly, for magnetosonic-like fluctuations, we have

$$\frac{\tau_{cascade}(k_\perp)}{\tau_{cascade}(k_{\|})} \simeq \left(\frac{k_{\|}}{k_\perp}\right)_I^2 << \left(\frac{k_{\|}}{k_\perp}\right)_I << 1$$

This model therefore implies that, for both modes, the cascade of magnetic fluctuation energy is much faster in directions quasi-perpependicular to $\mathbf{B}_o$ than in directions quasi-parallel to the background field. We thus predict that the cascade regime of electron-positron turbulence should display the same type of anisotropy as found in PIC simulations

of cascading whistler turbulence.[10], [11] But for fluctuations at similar wavenumbers, the model further implies that the ratio of the perp-versus-parallel cascade rates are much faster for the magnetosonic-like fluctuations, implying that magneotsonic-like turbulence should be more anisotropic than Alfvén-like turbulence.

A complete simulation of homogeneous turbulence should be run to at least $t = \tau_{cascade}$ to assure that the full late-time physics of the cascade has been captured. From Equations (4) and (5) we note that the cascade is a product of two factors which both have strong, but opposite, dependences on the wavenumber; errors in estimating the value of either the wavenumber or the fluctuating magnetic field energy density can yield an incorrect estimate for $\tau_{cascade}$. However, let us assume, as is often the case, that the reduced power spectrum displays a power-law dependence on wavenumber, e.g.,

$$\frac{|\delta \mathbf{B}(k_\perp)|^2}{B_o^2} \equiv \frac{\sum_{k_\parallel} |\delta \mathbf{B}(\mathbf{k})|^2}{B_o^2} = \epsilon (k_\perp c/\omega_e)^{-\alpha}$$

where ϵ characterizes the total energy in the spectrum. Then, for example, the cascade time for Alfvén-like fluctuations at quasi-perpendicular propagation becomes

$$\tau_{cascade}(k_\perp)|\Omega_e| \simeq \frac{\sqrt{2}\pi}{\epsilon} \frac{k_\parallel}{k_\perp} \left(\frac{k_\perp c}{\omega_e}\right)^{\alpha-3}$$

If, as we anticipate, $2 < \alpha < 4$ for turbulence in electron-positron plasmas, then this expression becomes relatively insensitive to the magnitude of the wavenumber and a more accurate estimate for $\tau_{cascade}$ may be obtained.

IV. INSTABILITIES

In this section, we return to linear theory to consider the consequences of the temperature anisotropy $T_{\perp j}/T_{\parallel j} > 1$ separately on the positrons and electrons. In an electron-proton plasma, this anisotropy on the protons leads to two distinct instabilities, the Alfvén-cyclotron instability with $0 < \omega_r < \Omega_{proton}$ and maximum growth rate at $\mathbf{k} \times \mathbf{B}_o = 0$ and the proton mirror instability with $\omega_r = 0$ in a homogeneous plasma and which grows only at propagation oblique to the background magnetic field. If $\beta_{proton} \sim 1$, these two modes have similar growth rates and threshold anisotropy conditions.[28] On the other hand, if $T_{\perp e}/T_{\parallel e} > 1$, the whistler anisotropy instability at $\Omega_{proton} < \omega_r < |\Omega_e|$ and maximum growth at $\mathbf{k} \times \mathbf{B}_o = 0$ has a far larger growth rate than the electron-driven mirror if $m_p >> m_e$.

In an electron-positron plasma $T_{\perp e}/T_{\|e} > 1$ can drive the magnetosonic-like mode unstable, just as a sufficiently large $T_{\perp p}/T_{\|p} > 1$ will lead to instability of the Alfvén-like mode. The relevant wave-particle interactions here are the cyclotron resonances, so we name these two growing modes the electron cyclotron and positron cyclotron instabilities, respectively. Figure 4 shows the dispersion of the electron cyclotron instability at three angles of propagation. By analogy with the whistler anisotropy instability, the maximum growth rate γ_m is at $\mathbf{k} \times \mathbf{B}_o = 0$ and $k_\| c/\omega_e \simeq 1$. For the same parameters except isotropic electrons and $T_{\perp p}/T_{\|p} = 3.0$, the positron cyclotron instability has identical dispersion properties. For both instabilities, $\gamma/|\Omega_j|$ increases with increasing species anisotropy and increasing $\beta_{\|j}$.

A $T_\perp/T_\|$ which is sufficiently greater than unity can also drive a compressible mirror instability with maximum growth highly oblique to $\mathbf{B}_o$. Figure 5 illustrates some dispersion properties of the positron mirror instability for a single choice of plasma parameters. The maximum growth rate lies at a wavevector strongly oblique (but not strictly perpendicular) to $\mathbf{B}_o$; increasing the anisotropy pushes γ_m to smaller values of θ. The positron compressibility is nonzero but relatively small; although C_e is not shown, $C_e \lesssim C_p$ for the parameters shown here. In contrast, Figure 5b shows that the magnetic compressibility is close to unity. Each of these properties is similar to those of the proton mirror instability in an electron-proton plasma. Sample computations show that, if the only change in the parameters is to transfer the positron anisotropy to the electrons, the growth rate of the electron mirror instability has exactly the same wavevector dependence as that of the positron mirror instability.

Figure 6 shows the threshold anisotropies at three different values of the maximum growth rate for the positron mirror instability (dotted lines) and the positron cyclotron instability (solid and dashed lines) as functions of $\beta_{\|p}$. The results are qualitatively similar to the thresholds for the analogous Alfvén-cyclotron and proton mirror instabilities in an electron-proton plasma; [28] at $\beta_{\|p} \lesssim 5$ the positron cyclotron instability has the smaller threshold anisotropy, whereas the positron mirror instability has the lower threshold if $\beta_{\|p}$ is sufficiently large and $\gamma_m/\Omega_p \leq 0.01$. However, in contrast to the electron-proton case, Figure 6 shows that, if the maximum growth rate is sufficiently large, the positron cyclotron instability has the lower threshold anisotropy over $1 \leq \beta_{\|p} \leq 100$.

V. CONCLUSIONS

We have used linear kinetic dispersion theory to study electromagnetic fluctuations in a magnetized, homogeneous, collisionless electron-positron plasma. There are two weakly damped electromagnetic modes: the incompressible Alfvén-like fluctuation and the magnetosonic-like fluctuation which becomes compressible at propagation oblique to the background magnetic field. The two modes have identical dispersion and damping at parallel propagation[18], where the onset of cyclotron damping is near $k_{\|}c/\omega_e \simeq 1$. Both modes have phase speeds ω_r/k which monotonically decrease with increasing wavenumber, so that neither mode exhibits whistler-like dispersion with $\omega \simeq k^2$. A sufficiently large $T_{\perp e}/T_{\|e}$ drives the electron cyclotron instability while a sufficiently large $T_{\perp p}/T_{\|p}$ excites the positron cyclotron instability with maximum growth rate in both cases at $\mathbf{k} \times \mathbf{B}_o = 0$ and $k_{\|}c/\omega_j \simeq 1$. The same anisotropies can also excite the electron mirror and positron mirror instabilities with maximum growth rate at propagation oblique to $\mathbf{B}_o$ and $kc/\omega_e < 1$.

Using our linear theory results and a basic turbulence model, we have made predictions concerning properties of homogeneous turbulence in electron-positron plasmas. We predict that cascading turbulence will be anisotropic in the same sense as MHD and whistler turbulence. However, in the absence of whistler-like dispersion, we further predict that there will be only a single regime of turbulent cascade with power-law spectra, followed by a true dissipation range of rapidly decreasing spectra at $kc/\omega_e \gtrsim 1$. These predictions now can be tested with PIC simulations in an electron-positron plasma model, while awaiting improvements in computing power and speed that will permit full-fledged PIC simulations of turbulence in electron-proton plasmas at some later date.

If these predictions are confirmed by PIC simulations in $m_p = m_e$ plasmas, the next step should be to extend the simulations to the range $1 < m_p/m_e \leq 1836$. At $m_p/m_e \simeq 64$, linear theory predicts that the characteristic $\omega_r \sim k_{\|}k$ dispersion of the whistler becomes distinct on the magnetosonic-like mode, as illustrated in Figure 7. Thus, PIC simulations of turbulence at sufficiently large m_p/m_e should, if the hypothesis of Reference [21] is correct, then yield cascading spectra with two distinct power law regimes separated by a breakpoint at $kc/\omega_{proton} \sim 1$. Such computations would also help resolve the current controversy as to whether short wavelength turbulence observed in the solar wind is primarily due to whistler modes at $\omega_r > \Omega_{proton}$[11] or to kinetic Alfvén fluctuat ions at $\omega_r < \Omega_{proton}$.[25], [26]

ACKNOWLEDGMENTS

The Los Alamos portion of this work was performed under the auspices of the U.S. Department of Energy (DOE). It was supported by the Magnetic Turbulence and Kinetic Dissipation Project of the Laboratory Directed Research and Development Program at Los Alamos, and by the Solar and Heliospheric Physics SR&T Program of the National Aeronautics and Space Administration. Work at UCSD was supported by NSF-GEM grant ATM-0802380.

---

* pgary@lanl.gov

† homakar@gmail.com

[1] D. Biskamp, Magnetohydrodynamic Turbulence (Cambridge University Press, New York, 2003).

[2] S. Oughton and W. H. Matthaeus, Nonl. Proc. Geophys., **12**, 299 (2005).

[3] S. Dastgeer, A. Das, P. Kaw, and P. H. Diamond, Phys. Plasmas **7**, 571 (2000).

[4] D. Biskamp, E. Schwartz, A. Zeiler, A. Celani, and J. F. Drake, Phys. Plasmas **6**, 751 (1999).

[5] J. Cho and A. Lazarian, Astrophys. J. **615**, L41 (2004).

[6] N. Bessho and A. Bhattacharjee, Phys. Plasmas, **14**, 056503 (2007).

[7] W. Daughton and H. Karimabadi, Phys. Plasmas, **14**, 072303 (2007).

[8] J. F. Drake, M. A. Shay, and M. Swisdak, Phys. Plasmas, **15**, 042306 (2008).

[9] L. Yin, W. Daughton, H. Karimabadi, B. J. Albright, K. J. Bowers, and J. Margulies, Phys. Re. Lett., **101**, 125001 (2008).

[10] S. P. Gary, S. Saito, and H. Li, Geophys. Res. Lett. **35**, L02104 (2008).

[11] S. Saito, S. P. Gary, H. Li, and Y. Narita, Phys. Plasmas, **15**, 102305 (2008).

[12] P. E. Hardee and W. K. Rose, Ap. J., **219**, 274 (1978).

[13] J.-I. Sakai and T. Kawata, J. Phys. Soc. Japan, **49**, 747 (1980).

[14] S. Matsukiyo and T. Hada, Phys. Rev. E, **67**, 046406 (2003).

[15] V. Munoz, T. Hada, and S. Matsukiyo, Earth Planets Space, **58**, 1213 (2006).

[16] S. Q. Liu, Y. L. Liao, X. L. Liu, Q. S. Xiao, and W. D. Zhang, J. Plasma Phys., **74**, 807 (2008).

FIG. 1: Linear dispersion properties of the Alfvén-like mode in electron-positron plasmas as functions of wavenumber with parameters as stated in Section II and angles of propagation as labeled. (a) The real frequency $\omega_r/|\Omega_e|$ and the damping rate $\gamma/|\Omega_e|$. (b) The parallel fluctuating electric field ratio $|\delta E_{||}|^2/|\delta\mathbf{E}|^2$. (c) The positron compressibility C_p.

FIG. 2: Linear dispersion properties of the magnetosonic-like mode in electron-positron plasmas as functions of wavenumber with parameters as stated in Section II and angles of propagation as labeled. (a) The real frequency $\omega_r/|\Omega_e|$ and the damping rate $\gamma/|\Omega_e|$. (b) The parallel fluctuating electric field ratio $|\delta E_{||}|^2/|\delta\mathbf{E}|^2$. (c) The electron compressibility C_e.

[17] P. Chang, A. Spitkovsky, and J. Arons, Ap. J., **674**, 378 (2008).

[18] N. Iwamoto, Phys. Rev. E, **47**, 604 (1993).

[19] S. P. Gary, *Theory of Space Plasma Microinstabilities* (Cambridge University Press, New York, 1993).

[20] S. P. Gary and J. E. Borovsky, J. Geophys. Res. **109**, A06105 (2004).

[21] O. Stawicki, S. P. Gary, and H. Li, J. Geophys. Res. **106**, 8273 (2001).

[22] D. Biskamp, E. Schwartz, and J. F. Drake, Phys. Rev. Lett. **76**, 1264 (1996).

[23] S. Galtier and A. Bhattacharjee, Phys. Plasmas **10**, 3065 (2003).

[24] C. W. Smith, K. Hamilton, B. J. Vasquez, and R. J. Leamon, Astrophys. J. **645**, L85 (2006).

[25] R. J. Leamon, C. W. Smith, N. F. Ness, W. H. Matthaeus, and H. K. Wong, J. Geophys. Res. **103**, 4775 (1998).

[26] G. G. Howes, S. C. Cowley, W. Dorland, G. W. Hammett, E. Quataert, and A. A. Schekochihin, J. Geophys. Res., **113**, A05103 (2008).

[27] H. Li, S. P. Gary, and O. Stawicki, Geophys. Res. Lett. **28**, 1347 (2001).

[28] S. P. Gary, S. A. Fuselier, and B. J. Anderson, J. Geophys. Res., **98**, 1481 (1993).

FIG. 3: Linear dispersion properties at $\mathbf{k}\times\mathbf{B}_o = 0$ of the Alfvén-like mode in electron-positron plasmas. Except for $\beta_{||p}$, parameters are as stated in Section II. Here the real frequency $\omega_r/|\Omega_e|$ (solid and dashed lines) and the damping rate $\gamma/|\Omega_e|$ (dotted lines) are shown as functions of wavenumber $k_{||}$ with $\beta_{||p}$ variations as labeled.

FIG. 4: Linear dispersion properties of the electron cyclotron instability with $T_{\perp e}/T_{\|e} = 3.0$ in electron-positron plasmas. All other parameters are as stated in Section II. The real frequency $\omega_r/|\Omega_e|$ and the growth/damping rate $\gamma/|\Omega_e|$ are shown as functions of the wavenumber for angles of propagation as labeled. At $\theta = 0^o$, the results are identical for the positron cyclotron instability with $T_{\perp p}/T_{\|p} = 3.0$.

FIG. 5: Linear dispersion properties of the positron mirror instability as functions of the direction of propagation in electron-positron plasmas. Panel (a) shows the growth rate and the positron compressibility, whereas panel (b) shows the magnetic compressibility as functions of θ. Parameters are as stated in Section II and as given in panel (b).

FIG. 7: The real frequency of the magnetosonic-like mode in a two-species plasma as a function of wavenumber at $\theta = 0^o$. The mass ratio m_p/m_e is varied as labeled; other parameters are as stated in Section II.

FIG. 6: Threshold positron anisotropies as functions of $\beta_{\|p}$ for three different values of the maximum growth rate of the positron cyclotron instability (solid and dashed lines) and the positron mirror instability (dotted lines). Other parameters are as stated in Section II.

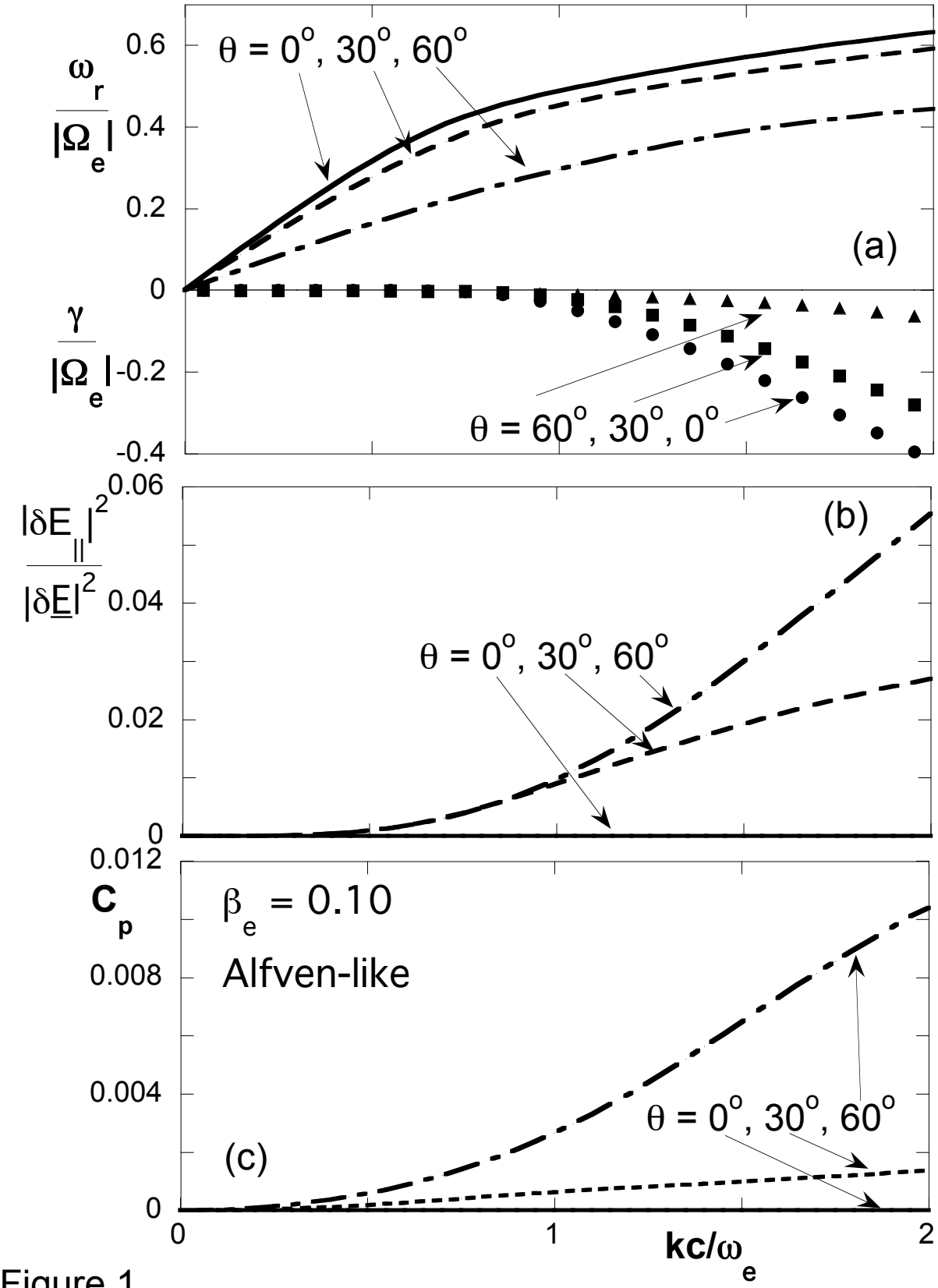
θ = 0°, 30°, 60°
ω_r / |Ω_e|
γ / |Ω_e|
θ = 60°, 30°, 0°
(a)
|δE_||^2 / |δE|^2
(b)
θ = 0°, 30°, 60°
C_p
β_e = 0.10
Alfven-like
θ = 0°, 30°, 60°
(c)
kc/ω_e

Figure 1

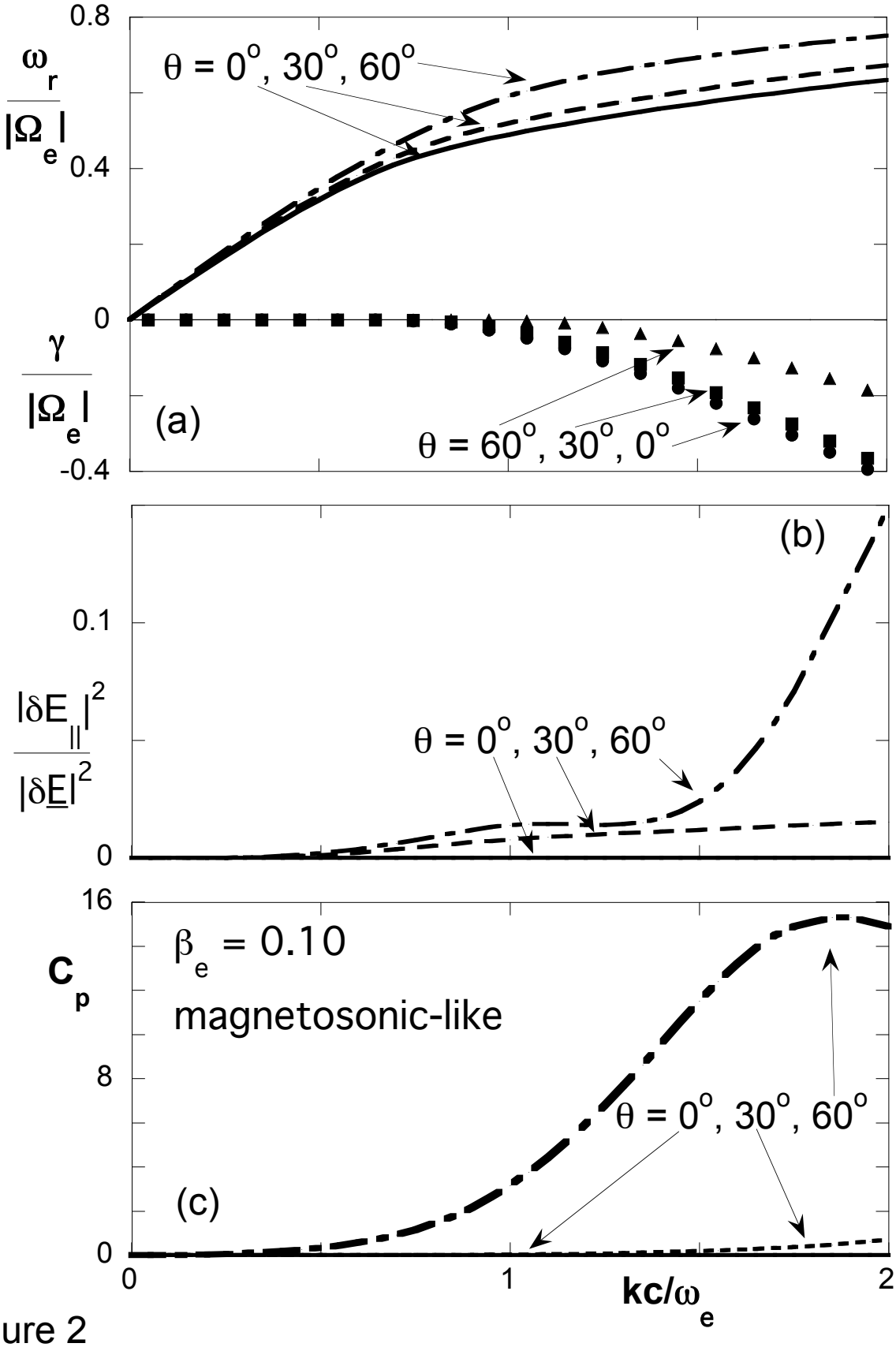
0.8
$\frac{\omega_r}{|\Omega_e|}$
0.4
0
$\frac{\gamma}{|\Omega_e|}$
-0.4
θ = 0°, 30°, 60°
θ = 60°, 30°, 0°
(a)
(b)
0.1
$\frac{|\delta E_{||}|^2}{|\delta \underline{E}|^2}$
0
θ = 0°, 30°, 60°
16
C_p
β_e = 0.10
magnetosonic-like
8
θ = 0°, 30°, 60°
(c)
0
0
1
2
kc/ω_e

Figure 2

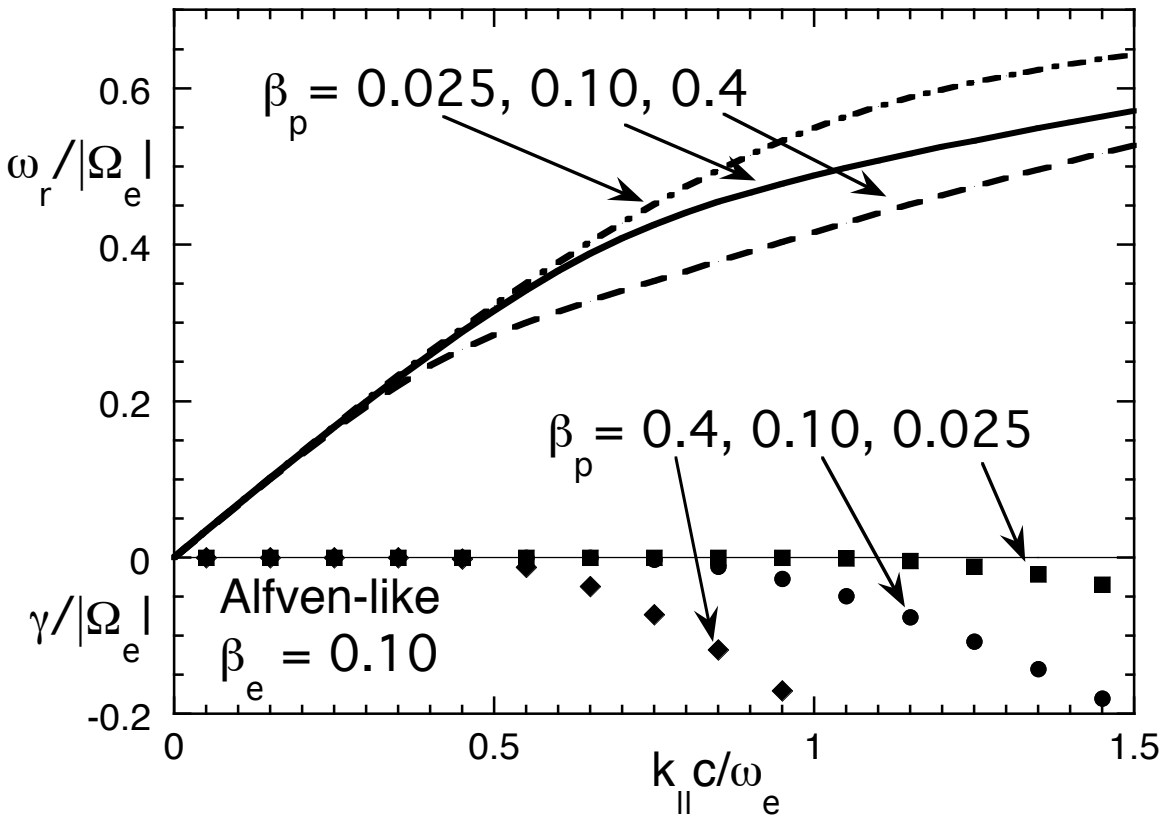
β_p = 0.025, 0.10, 0.4
β_p = 0.4, 0.10, 0.025
Alfven-like
β_e = 0.10
$\omega_r/|\Omega_e|$
$\gamma/|\Omega_e|$
$k_{\parallel}c/\omega_e$
0.6
0.4
0.2
0
-0.2
0
0.5
1
1.5

Figure 3

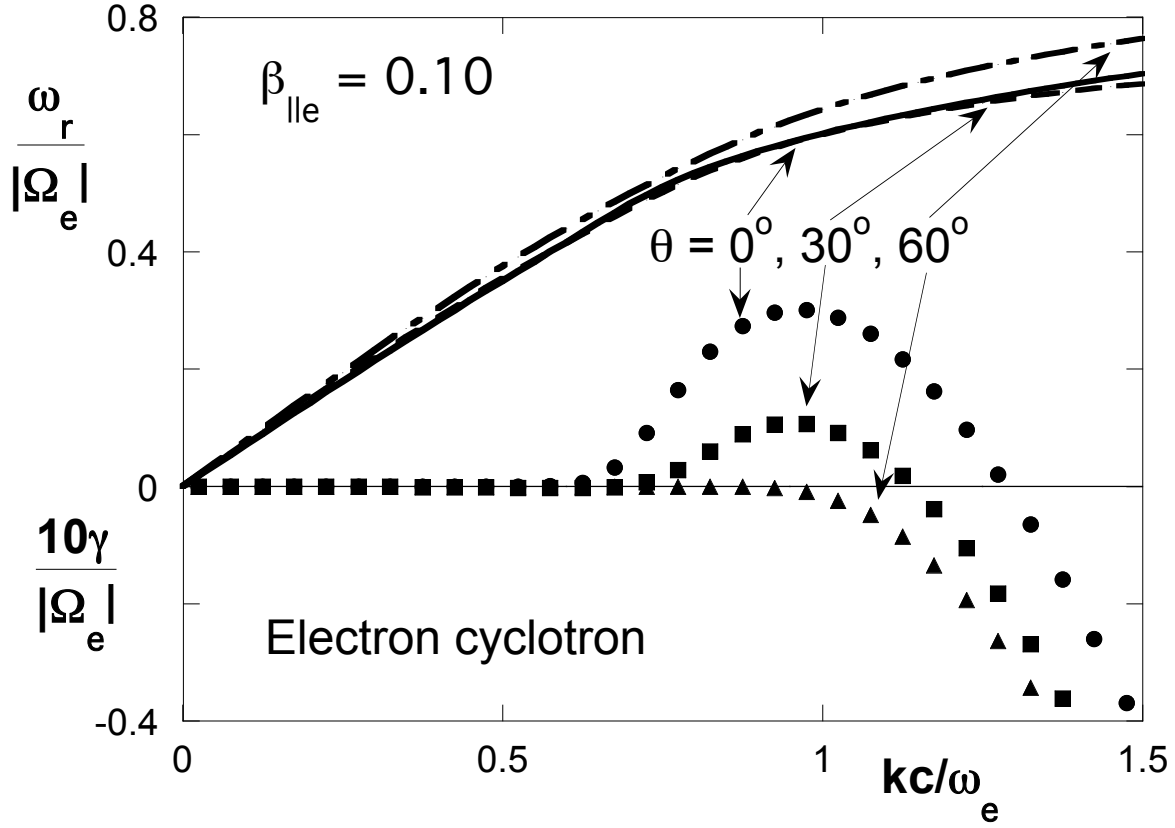
0.8
0.4
0
-0.4
$\frac{\omega_r}{|\Omega_e|}$
$\frac{10\gamma}{|\Omega_e|}$
$\beta_{\parallel e}$ = 0.10
θ = 0°, 30°, 60°
Electron cyclotron
0
0.5
1
1.5
kc/ω_e

Figure 4

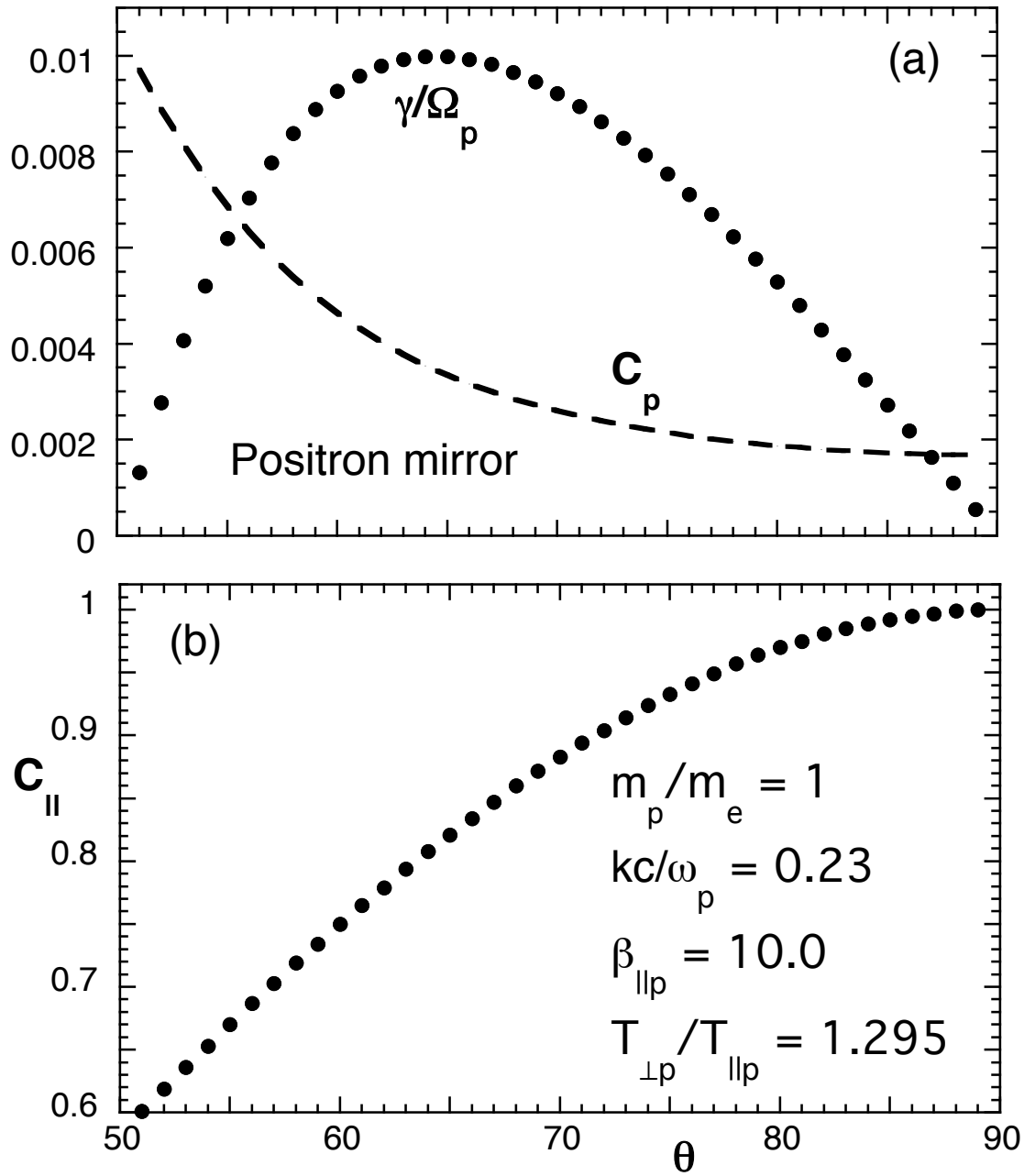
(a)
0.01
0.008
0.006
0.004
0.002
0
γ/Ω_p
C_p
Positron mirror
(b)
1
0.9
0.8
0.7
0.6
C_II
m_p/m_e = 1
kc/ω_p = 0.23
β_IIp = 10.0
T_⊥p/T_IIp = 1.295
50
60
70
80
90
θ

Figure 5

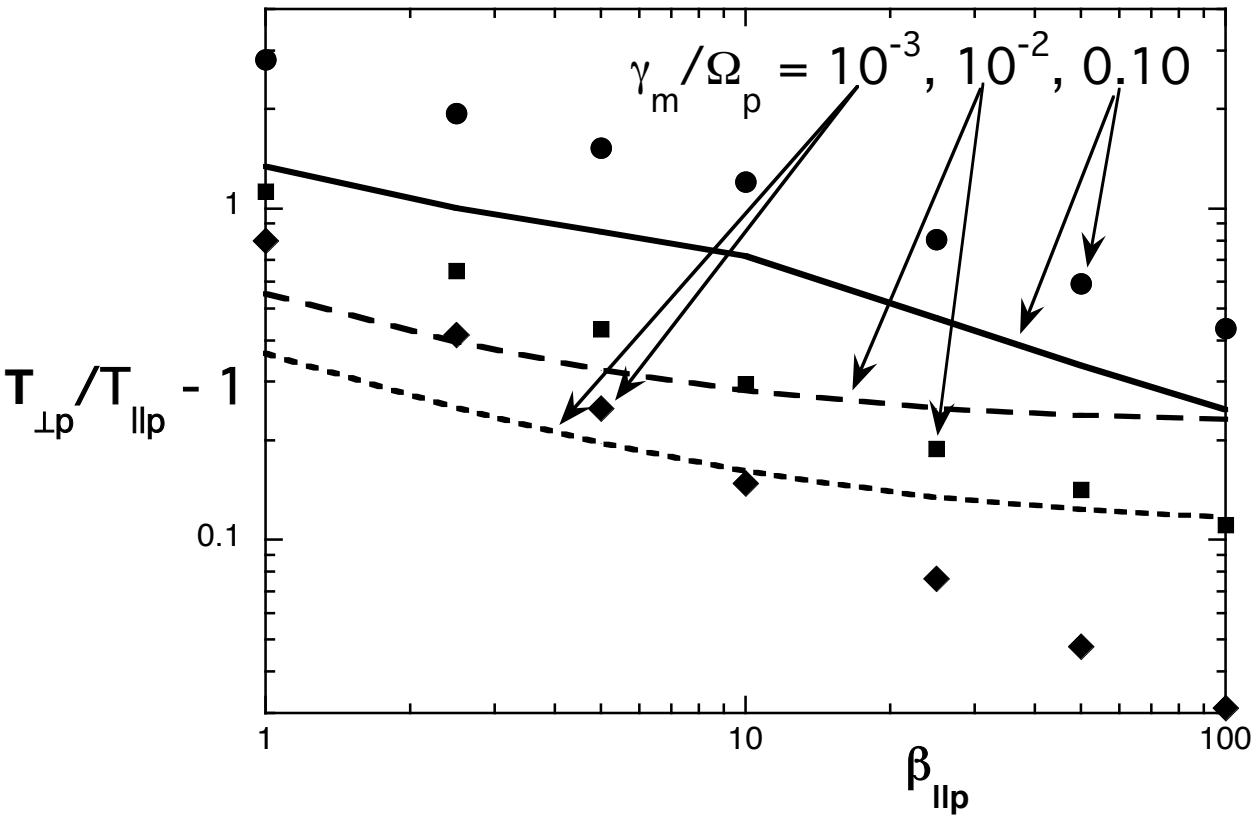
$\gamma_m/\Omega_p = 10^{-3}, 10^{-2}, 0.10$
$T_{\perp p}/T_{\parallel p} - 1$
1
0.1
1
10
100
$\beta_{\parallel p}$

Figure 6

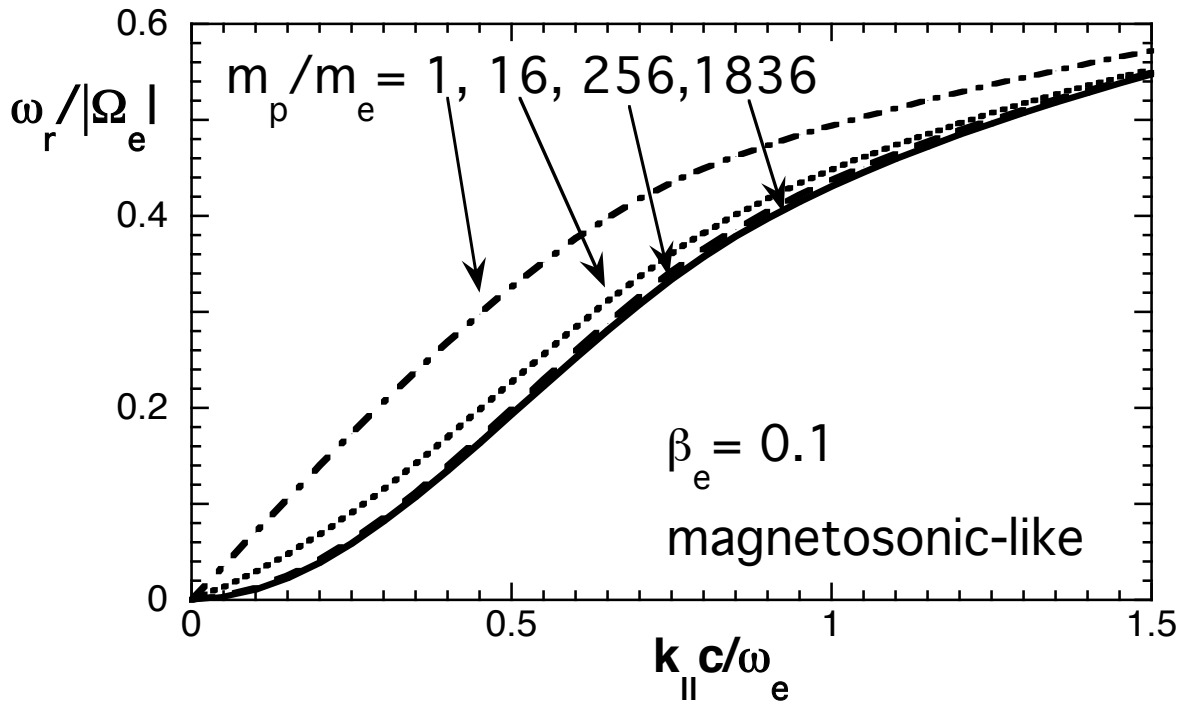
0.6
0.4
0.2
0
0
0.5
1
1.5
$\omega_r/|\Omega_e|$
$k_{\parallel}c/\omega_e$
m_p/m_e = 1, 16, 256,1836
β_e = 0.1
magnetosonic-like

Figure 7